Electrochimica Acta 87 (2013) 739–748

Contents lists available at SciVerse ScienceDirect

Electrochimica Acta

journal homepage: www.elsevier.com/locate/electacta

Electrochemical study of copper chloride complexes in the RTIL 1-butyl-1-methylpyrrolidinium bis(trifluoromethylsulfonyl)imide

Tuomas Vainikka [a], David Lloyd [a], Lasse Murtomäki [a,*], José A. Manzanares [a,b], Kyösti Kontturi [a]

[a] Aalto University, Department of Chemistry. PO Box 16100, 00076 Aalto, Finland
[b] University of Valencia, Faculty of Physics, Department of Thermodynamics, c/Dr. Moliner, 50, E-46100 Burjasot, Spain

ARTICLE INFO

Article history:
Received 13 June 2012
Received in revised form
21 September 2012
Accepted 21 September 2012
Available online xxx

Keywords:
Ionic liquid
Pyrrolidinium
Copper chloride complex
Tsallis thermostatistics
Transport equations

ABSTRACT

The electrochemistry of copper(I) and copper(II) chloride complexes in the RTIL 1-butyl-1-methylpyrrolidinium bis(trifluoromethylsulfonyl)imide, $BMPTf_2N$, has been studied with constant current electrolysis and cyclic staircase voltammetry at temperatures between 21.0 and 96.0 °C and in different concentrations of chloride. The chloride concentration was controlled by addition of 1-butyl-1-methylpyrrolidinium chloride, BMPCl. An important finding is the evidence of a three-coordinated complex, $Cu(I)Cl_3^{2-}$ which has not been found in organic chloroaluminates without a significant increase in temperature. Two Cu(I) species were found at molar ratios of $[Cl^-]/[Cu] < 4$. The kinetic parameters for the quasi-reversible Cu(I)–Cu(II) electron transfer were obtained with non-linear fitting. Successful fits required that the charge transfer coefficients for the reduction of Cu(II) (α) and oxidation of Cu(I) (β) did not sum up to unity, i.e. $\alpha + \beta \neq 1$. This result was interpreted using Tsallis non-extensive thermostatistics.

1. Introduction

1-Butyl-1-methylpyrrolidinium bis(trifluoromethylsulfonyl) imide, $BMPTf_2N$, is an air and moisture stable hydrophobic room temperature ionic liquid, RTIL. It was first investigated by MacFarlane et al. [1] for its physical properties, including phase transition temperature, viscosity, density and conductivity. Also, the electrochemistry and deposition of Si [2,3], Al [4,5], Ta [6], Se, In and Cu [7] in $BMPTf_2N$ has been reported. In these cases, chloride salts were used without additives as the source of metal ions with the exception of Ta, where the experiments were carried out in the presence and absence of LiF as an additive. Metal salts with inorganic anions have limited solubility in RTILs based on fluorinated anions. Two different approaches to improve their solubility have been reported in the literature: addition of a complexing agent with components common to both the RTIL and the inorganic salt [8], or using a salt which has a common anion with the RTIL [9].

The electrochemistry of copper(I) and copper(II) chloride complexes has been thoroughly investigated in the chloroaluminate ionic liquids. Hussey et al. [10] reported that the reduction of Cu(II) is reversible, and that the reduction of Cu(I) to metallic Cu proceeds through instantaneous three-dimensional nucleation in the acidic $AlCl_3^-$ butylpyridinium chloride IL. Also nernstian slopes were obtained by varying the ratio of [Cu(II)] to [Cu(I)], suggesting that these cations are not complexed with chloride ions in acidic compositions. Nanjundiah and Osteryoung [11] utilized both the Lewis acidic and Lewis basic regimes of the same IL, and found evidence of $Cu(I)Cl_4^{3-}$ and $Cu(II)Cl_6^{4-}$ in the Lewis basic regime using potentiometric measurements. Laher and Hussey [12] reported the equilibrium between $Cu(I)Cl_2^-$, $Cu(I)Cl_3^{2-}$, and $Cu(I)Cl_4^{3-}$ in the Lewis basic $AlCl_3^-$ 1-ethyl-3-methylimidazolium chloride IL. They found that 2 and 4 coordinated complexes would dominate at 40 °C, but the equilibrium shifts toward a 3 coordinated complex when the temperature is raised.

Our previous research on the Cu^{2+} electrochemistry [13] has shown that there could be two species present in homogenous equilibrium in $BMPTf_2N$ with added BMPCl. At relatively low concentrations of chloride, approximately 1:1 molar ratio of BMPCl and $Cu(II)Cl_2$, cyclic voltammetry would show two separate Cu^{2+} reduction waves at potentials positive to Cu deposition on Pt. Raising the temperature did not change the relative magnitudes of these waves, but the shape of the wave at the lower potential was changed drastically. As the chloride content was increased, the wave at the higher potential, which showed no change with respect to temperature apart from obvious effects, would vanish, leaving just the wave at the lower potential. The same behavior will be seen further in this paper, as the redox processes are measured by oxidation of Cu(I).

Electrochemical measurements in $Cu(II)Cl_2$ solutions with minimal added chloride are quite hard to quantify because $Cu(II)Cl_2$ can

* Corresponding author. Tel.: +358 9 470 22585; fax: +358 9 470 22580.
E-mail address: lasse.murtomaki@aalto.fi (L. Murtomäki).

0013-4686/$ – see front matter © 2012 Elsevier Ltd. All rights reserved.
http://dx.doi.org/10.1016/j.electacta.2012.09.062

Table 1
Prepared electrolyte solutions. The copper mass fraction was determined by AAS analysis (Varian 240, air–acetylene flame, λ = 324.8 nm). The total chloride content was determined by mass assuming a weighing accuracy of 1 mg. A density of 1.41 g/cm^3 for $BMPTf_2N$ [1] was used to calculate the concentrations.

Solution	Concentration (mM)	mg(Cu)/mg	
	total [Cl^-]	[Cu(II)]	[Cu(I)]
Cl^- a	77 ± 2		
Cl^- b	184 ± 2		
Stock Cu(II)	397 ± 3	46 ± 1	2.07 ± 0.04
Low Cu(II)	397 ± 3	51 ± 1	2.32 ± 0.02
Low Cu(I)	399 ± 3	45 ± 2	2.05 ± 0.07
High Cu(I) a	392 ± 2	92 ± 2	4.17 ± 0.08
High Cu(I) b	435 ± 2	92 ± 2	4.15 ± 0.09
High Cu(I) c	480 ± 2	93 ± 2	4.21 ± 0.08

be dissolved only by complexation with chloride. Such solutions are turbid, thus the concentration of the electroactive species is unknown. The electrochemical study presented in this paper starts from the Cu(I) species which, at the chloride contents considered, do not have the same solubility problems as $Cu(II)Cl_2$.

Since even tiny amounts of atmospheric oxygen or moisture change the behavior of the system, i.e. introduce additional reaction mechanisms and complex equilibria, the measurements are preferably carried out in an inert atmosphere of a glove box. When metals are to be deposited electrochemically from RTILs, the reduction potential may also depend on the complex speciation. The purpose of this work is to study further the different copper chloride complexes and elucidate the kinetics of the prevailing reactions.

2. Experimental

2.1. Reagents and solutions

The chemicals used were Cu(II) chloride (Alfa Aesar, 99.995%, ultra dry, sealed ampoule), 1-butyl-1-methylpyrrolidinium chloride (Fluka, ≥99.0%) (BMPCl), 1-butyl-1-methyl-pyrrolidinium bis(trifluoromethylsulfonyl)imide (Fluka, ≥98.5%) ($BMPTf_2N$). Three sets of solutions were prepared in a glove box (Vacuum Atmospheres Company) under argon atmosphere which was circulated through a gas purifier. An opened jar of P_2O_5 was kept inside the glove box to further remove water from the inert gas. The oxygen and water contents were both found to remain below 2 ppm. First, for the study of chloride only, two solutions containing 77 ± 2 mM and 184 ± 2 mM BMPCl in $BMPTf_2N$ were prepared by mixing after several hours with a magnetic stirrer, yielding clear solutions.

For the electrochemical study of copper chloride complexes, a second set of solutions with a molar ratio of ca. 8 of total chloride to total copper, and a third set with three different molar ratios of 4–5 of total chloride to Cu(I), were prepared from a stock solution of Cu(II) that was made by mixing $BMPTf_2N$, BMPCl and $Cu(II)Cl_2$. The stock solution was mixed vigorously for several hours, during which it turned yellow. Cu(I) electrolytes were prepared from a portion of the stock solution by the addition of 5 mm long, 5 mm diameter Cu slugs lathed from a 9 mm diameter copper rod (Koch-Light, ≥99.95%). The solution turned colorless during ca. 24 h under vigorous mixing. The final Cu(I) concentration is assumed to be a result of complete comproportionation,

$$Cu^{2+} + Cu \rightarrow 2Cu^{+} \quad (1)$$

that is, twice the starting Cu(II) concentration. The stock solution had the concentration ratio of Cl^- to total Cu of ca. 8. The comproportionation reaction obviously brought this ratio down to ca. 4 by doubling the Cu concentration (see Table 1). Thus, in order to make a Cu(I) electrolyte with similar molar ratio of Cl^- to total Cu as the stock solution, a portion of the comproportionated solution was diluted with a mixture of BMPCl and $BMPTf_2N$. This solution is referred to as the "Low Cu(I) solution". The rest of the comproportionated solution was divided in three portions, to which two of them BMPCl was added to modify the chloride content. As the Cu(I) concentration was not reduced by dilution for these solutions, they are referred to as the "High Cu(I) solutions".

The stock solution was used in the first experiments, but it was found that Cu(II) was gradually reduced to Cu(I). The Cu(I) solutions did not exhibit the same behavior. Thus, a fresh Cu(II) solution was made in the same way as the stock solution. The new Cu(II) solution is referred to as the "Low Cu(II) solution". Table 1 holds a summary of the electrolytes described above.

2.2. Apparatus

The electrochemical experiments were carried out in the same glove box where the electrolytes were prepared. A three-electrode setup was mainly used, and modifications to this setup will be clarified in the corresponding experimental sections. A (1.00 ± 0.01) mm diameter Pt disc was used as a working electrode. The diameter was measured with a microscope. Some of the experiments utilize a reference electrode consisting of a 0.7 mm diameter Cu wire inside a glass capillary that has a narrow opening separating the reference electrolyte from the bulk electrolyte. However, due to its high impedance, this capillary electrode was not utilized in most of the measurements, but it was used to calibrate a wire reference electrode in direct contact with the electrolyte.

Galvanostatic experiments in all Cu(I) electrolyte solutions and potentiostatic experiments in the High Cu(I) solutions were conducted with the Autolab PGSTAT302N controlled with GPES software. The cyclic staircase voltammetry (CSV) responses in the Low Cu(I) and Low Cu(II) solutions were measured at different temperatures using a Princeton Applied Research Model 263A potentiostat. The *iR* drop was compensated for by positive feedback. In order to determine the solution resistance, a EG&G Princeton Applied Research Model 5208 Dual Lock-In Amplifier was attached to the PAR 263A potentiostat, and a 10 kHz sine wave of 10 mV(RMS) amplitude was applied to the cell. The real part of the impedance was assumed to be a sufficient approximation of the solution resistance, and it was compensated for at least 75%, current range permitting.

The temperature was controlled with a Supercool PR-59 Peltier controller attached to a specially constructed heating–cooling-module. The module utilized a 60 W Peltier element, which was sandwiched between an aluminum CPU cooler (cold side) and a block of copper (hot side). An aluminum cylinder attached to the hot side with a heat-conducting adhesive worked as a mantle for the glass vial containing the electrolyte. A glass-bead 10 kΩ NTC resistor inside the copper block on the hot side was used for the Peltier controller feedback circuitry, but the actual temperature inside the electrolyte vial was measured with a J-type thermocouple inside a glass sheath. The thermocouple voltage was amplified using an AD594 monolithic thermocouple amplifier IC with internal cold junction compensation.

3. Results and discussion

3.1. Cu(I) oxidation in the High Cu(I) solutions

The CSV responses in the High Cu(I) electrolytes were measured using a Cu wire as a reference electrode and a copper coil as an auxiliary electrode. The copper wire reference potential was corrected against the capillary reference filled with the High Cu(I) a electrolyte. The correction was 3 mV against the High Cu(I) a electrolyte (itself), and 15 mV against the High Cu(I) b and c electrolytes.

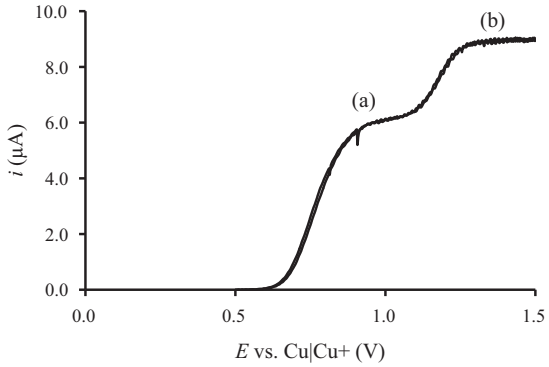

Fig. 1. Steady-state response recorded in the High Cu(I) a solution containing 392 mM of total chloride. Scan rate is 1 mV/s.

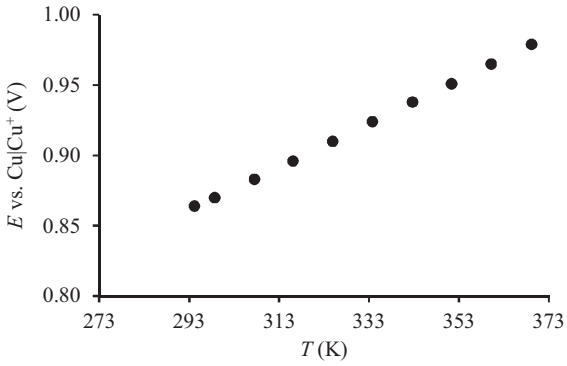

Fig. 3. Temperature dependence of the Pt pseudo-reference measured in the Low Cu(II) electrolyte against the capillary reference filled with the Low Cu(I) electrolyte.

The true starting and switching potentials were adjusted in line with the measured corrections for each electrolyte solution.

The "steady-state" curve (CSV at 1 mV/s) of Cu(I) oxidation, measured under vigorous stirring using a magnetic stirrer, shows two waves (Fig. 1), the second one at ca. 1.2 V (b) being 50% lower than the first one at ca. 0.8 V (a). This result seems rather difficult to explain, because if there was only one Cu(I) species undergoing second oxidation from Cu(II) to Cu(III), the limiting current (b) would be twice the limiting current (a). The separate waves must, therefore, correspond to two Cu(I) complexes. The equilibrium between these complexes has to settle, however, rather slowly, because we see two waves, i.e. within the time frame of the experiment hardly no change in their relative concentrations apparently takes place. If there was a facile homogeneous equilibrium between the two Cu(I) complexes, only a single oxidation wave would be seen. A finite element simulation was done assuming that the two complexes differ by one chloride, and, indeed, a curve similar to Fig. 1 could be recovered (see Appendix A). These simulations are not, however, able to resolve the composition of the complexes.

The oxidation of Cu(I) was studied further with cyclic voltammetry (CSV) using all three High Cu(I) solutions. The CSV responses were recorded using 1 mV steps at the scan rates of 50, 100 and 200 mV/s from 0.25 V to 1.5 V. Also, voltammograms of a plain chloride solution are shown to prove that the wave at ca. 1.2 V is not due to chloride oxidation. As can be seen in Fig. 2, the oxidation wave at ca. 1.2 V is suppressed by increasing the total chloride concentration. Neither cathodic nor anodic peak potentials coincide, which rules out adsorption and supports the existence of a diffusing species. Hence, we suggest equilibrium

$$Cu(I)Cl_2^- + Cl^- \leftrightarrow Cu(I)Cl_3^{2-} \quad (2)$$

which agrees with the observation that adding chloride in the solution removes one of the complexes. The stoichiometry of the complexes still remains unknown and reaction (2) must be considered just as a reasonable suggestion. Since docking more chlorides into the complex probably changes its conformation, and since the diffusion coefficient of Cl^- in this IL is lower than those of the Cu complexes, as shown later on, the rate of reaction (2) can be, indeed, quite low.

3.2. Cyclic staircase voltammetry of the Low Cu(I) and Low Cu(II) solutions

The fact that one of the copper chloride species can be suppressed with a sufficient addition of chloride enables the quantification of the remaining electron transfer process. The Low Cu(I) and Low Cu(II) electrolytes were used to determine the cyclic staircase voltammetry (CSV) response of the Cu(I)–Cu(II) electron transfer as a function of temperature and scan rate. Using a step size of 10 mV, scan rates of 10, 20, 30, 50, 100, 200, 300, 500, and 1000 mV/s were measured at temperatures 21.0, 25.5, 34.4, 42.9, 51.8, 60.6, 69.5, 78.2, 87.0, and 96.0 °C. In the Low Cu(I) electrolyte, a copper coil was used as a counter electrode and a copper wire as a reference electrode, whereas in the Low Cu(II) electrolyte, both the counter and the reference electrodes were made of platinum, with the same physical dimensions as their copper counterparts. Thus, the Cu(II) measurements were made with a platinum pseudo-reference, which was offset afterwards for all temperatures by measuring its potential relative to the capillary reference filled with the Low Cu(I) electrolyte (Fig. 3). The determination of the offset was made separately and quickly to avoid excessive crossover between the reference electrolyte and the bulk electrolyte. The temperature dependence is fairly linear over the whole temperature range. The potentials in Fig. 3 are used to correct for the potential scale in all Low Cu(II) measurements, which appears as a drift of vertex potentials in Fig. 6. The measured CSVs and their corresponding fits at 25.5 °C and 96.0 °C are shown in Figs. 4 and 5. Fig. 6 shows the CSVs at 1 V/s in all the measured temperatures.

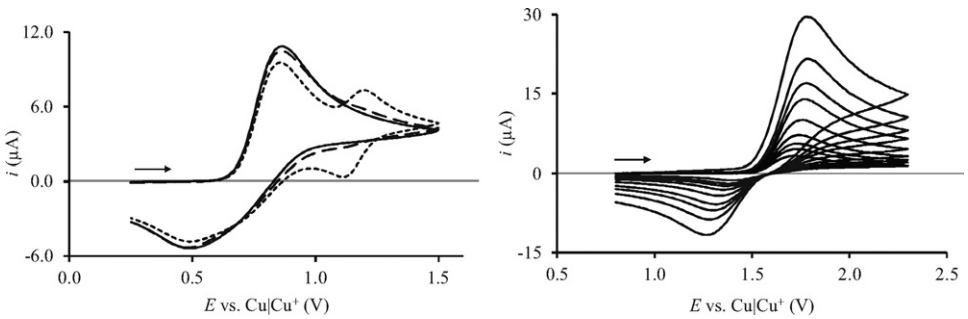

Fig. 2. Left: Cyclic voltammograms of three High Cu(I) electrolytes with total chloride concentrations of 392 mM (- - -), 435 mM (— — —), 480 mM (——), scan rate is 0.05 V/s. Right: Only 77 mM Cl^-, scan rate is 0.01, . . ., 1.0 V/s.

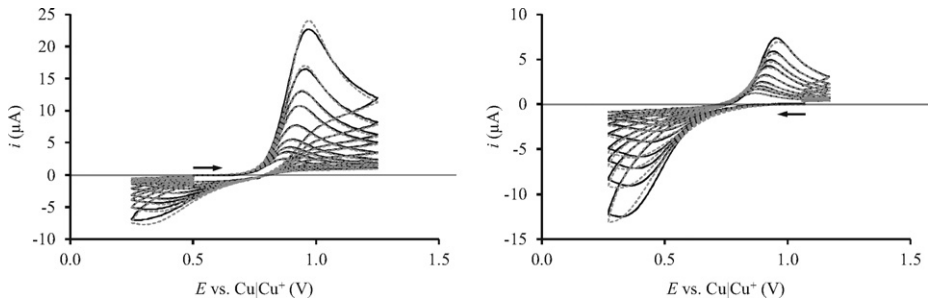

Fig. 4. CSVs for Cu(I) oxidation (left) and Cu(II) reduction (right) at 25.5 °C. Experimental data: black solid line; fitted data: gray dashed line; $\nu = 10, \ldots, 1000$ mV/s.

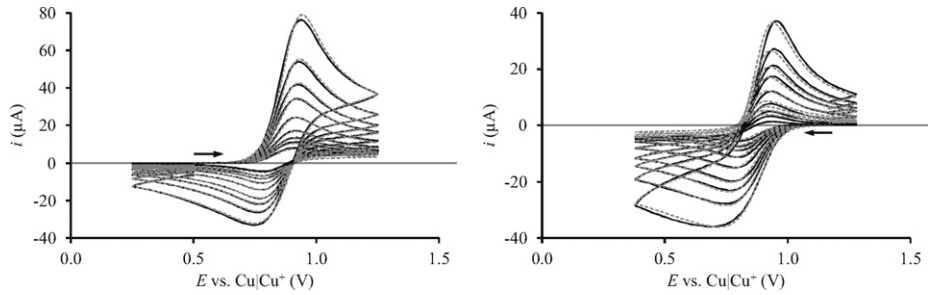

Fig. 5. CSVs for Cu(I) oxidation (left) and Cu(II) reduction (right) at 96.0 °C. Experimental data: black solid line; fitted data: gray dashed line; $\nu = 10, \ldots, 1000$ mV/s.

The temperature dependence of the cathodic peak potential corresponding to the reduction of Cu(II) shows a very strong shift of ~500 mV, contrary to the oxidation of Cu(I), which merely increases in magnitude as the temperature is increased. This is an indication of strongly asymmetrical electron transfer (i.e. apparent $\alpha \neq 0.5$).

Simulation of cyclic staircase voltammetry requires some explanation. In modern potentiostats a linear scan is approximated with small potential increments, ΔE, at small time intervals, Δt. According to our experience, the smaller ΔE is, the noisier is the current signal. When measurements are made in a glove box, the potentiostat usually resides outside, forcing to use long wires. Since the glove box is not an ideal environment for electrochemical measurements due to noise, it can thwart the success of a transient measurement, which requires fast potential control. Yet another source of noise is *iR* compensation with positive feedback, which is unavoidable in ILs of low conductivity. To achieve reliable potential control, larger potential steps must be applied, which, if the same 'scan rate' is concerned, reduces the rate at which the potential is updated. This enables the circuit to bypass transients in the beginning of a potential step, where the variation of the non-faradaic currents produced by capacitances in the long wiring and the double layer are at their highest. Updating the potential at this transient makes the read current both unstable and undefined. Although an increase in step size alleviates these problems, it seriously undermines the interpretation of peak currents and potentials with known theories of true linear voltammetry [14,15].

The theory of staircase voltammetry is discussed thoroughly in the literature for both reversible and quasi-reversible electrode kinetics [16,17]. Digital simulation of cyclic staircase voltammograms (CSV) has also been reported [18]. A successful analysis requires a simultaneous match of the experimental peak potentials and peak currents to their corresponding working curves. Since in staircase voltammetry, contrary to linear sweep voltammetry or CV, the peak potential is a rather poorly defined quantity [16], the entire CSV was fitted to the experimental data using the Levenberg–Marquardt algorithm. A simulation program was written in C [19,20], where mass transfer is described in a semi-infinite domain according to Fick's 2nd law as usual. Orthogonal collocation (OC) [21] was used in the simulations, approximating the concentration profile with an *N*th order Legendre polynomial. For the sake of flexibility, *N* could take values between 0 and 50. In OC, polynomials of an order as low as $N = 9$ can be used without a significant loss of accuracy. For the time integration, the Runge–Kutta–Fehlberg fourth-(fifth-) order algorithm, with an adaptive time step was used [22]. An arbitrary potential step function $E(t)$ was applied, the values of which were stored in a vector along their points of time. Integration between the data points in time was done with shorter time steps adjusted by the Fehlberg4(5) integrator, which means oversampling in the time

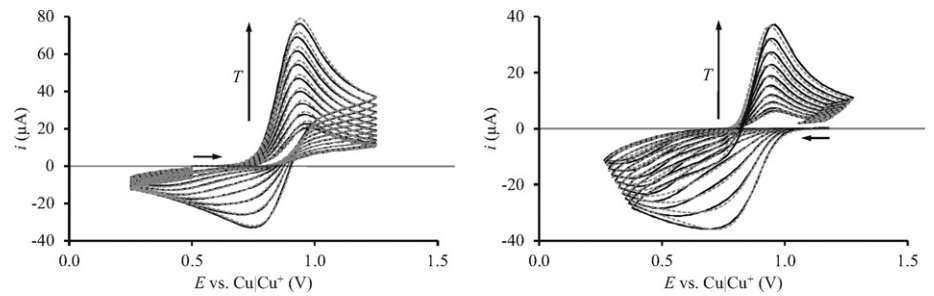

Fig. 6. CSVs for Cu(I) oxidation (left) and Cu(II) reduction (right) at $\nu = 1$ V/s. Experimental data, black solid line, fitted data, gray dashed line; $T = 21.0, \ldots, 96.0$ °C. Current increases with temperature.

Table 2
Fitted parameters at different temperatures. The errors are sums of the inaccuracies of bulk concentration (±2 mM), electrode radius (±10 μm), and temperature (±1 K). E_a is the activation energy and B the frequency factor.

T (K)	$D_{Cu(II)}$ (10^{-7} cm^2 s^{-1})	$D_{Cu(I)}$ (10^{-7} cm^2 s^{-1})	k^0 (10^{-4} cm s^{-1})	α	β	$E^{0\prime}$ (mV)
294.2	0.47 ± 0.07	0.9 ± 0.2	0.19 ± 0.02	0.226	0.523	733.6
298.7	0.56 ± 0.09	1.1 ± 0.2	0.25 ± 0.02	0.226	0.541	739.3
307.5	0.8 ± 0.1	1.5 ± 0.3	0.40 ± 0.03	0.226	0.570	746.7
316.1	1.1 ± 0.2	2.2 ± 0.4	0.67 ± 0.05	0.220	0.597	756.2
324.9	1.5 ± 0.2	3.1 ± 0.5	1.1 ± 0.1	0.208	0.621	766.8
333.8	2.0 ± 0.3	4.3 ± 0.7	2.0 ± 0.2	0.189	0.635	778.2
342.7	2.6 ± 0.4	6 ± 1	3.5 ± 0.3	0.167	0.644	791.2
351.3	3.4 ± 0.5	8 ± 1	6.0 ± 0.5	0.146	0.654	804.1
360.2	4.3 ± 0.7	10 ± 2	10.4 ± 0.8	0.125	0.666	817.9
369.1	5.4 ± 0.9	12 ± 2	17 ± 1	0.111	0.673	833.1
Errors				±0.002	±0.003	±0.3
E_a kJ/mol	29.7 ± 0.1	32.0 ± 0.2	54.2 ± 1.5			
B	(8.8 ± 0.5) ×10^{-3} cm^2 s^{-1}	(4.4 ± 0.4) ×10^{-2} cm^2 s^{-1}	(7 ± 4) × 10^4 cm s^{-1}			

domain. If oversampling were omitted, current between the onset of the potential step and the sampling point of the current would not be integrated, resulting in erroneous data. Our method is very similar to the COOL algorithm [23,24] which also utilizes the full curve. But, contrarily to the COOL algorithm, it does not ignore the background current, determines the goodness of fit from the examination of a variance–covariance matrix, and can fit multiple unweighted data sets of data in one go.

Since it is plausible that also Cu(II) has more than one chloride complexes in the solution, the possibility of homogeneous reactions in the simulations was considered. Numerous attempts were made to fit the data to varying models. Only with the Scheme-of-Squares shown in Scheme 1 it was possible to find at each temperature a set of parameters which was able to reproduce the measured voltammograms. Yet, the temperature and scan rate dependence of the parameters made no sense; hence also this scheme was rejected. In the case of High Cu(I), it was indirectly proved that the rate of the homogeneous chemical reaction (2) is quite low. Therefore, when performing 'potential scans' at rates significantly higher than that in Fig. 1, it is reasonable to assume that homogeneous reactions in the Scheme-of-Squares are not sensed at all. Consequently, the final fits were carried out ignoring the homogeneous reactions.

Although Figs. 4–6 show separately the CSVs for Cu(I) and Cu(II) at each temperature, all the data recorded at different scan rates for both Cu(I) and Cu(II) is fitted simultaneously. The fitted coefficients are shown in Table 2, and the corresponding Arrhenius plots are shown in Fig. 7. It was necessary to allow separate charge transfer coefficients α and β for oxidation and reduction, i.e. $\alpha + \beta \neq 1$. This became apparent when fitting oxidation and reduction waves separately. The kinetic current i thus is

$$-\frac{i}{FAk^0} = C_O^s e^{-\alpha f\eta} - C_R^s e^{\beta f\eta} \tag{3}$$

where O and R are the respective subscripts for the oxidized and the reduced species; C is the concentration, k^0 is the heterogeneous rate constant, A is the electrode area. The potential with respect to the standard potential is $\eta = E(t) - E^{0\prime}$, and superscript '$s$' denotes the concentration at the surface. The meaning of the diffusion coefficients is discussed in the Appendix A.

The fact that the simulation of the experimental voltammograms requires the use of transfer coefficients such that $\beta \neq 1-\alpha$ can be considered as an indication that the Boltzmann equilibrium distribution, which can be retrieved from the Butler–Volmer equation at zero current, does not describe accurately the ionic distributions. This fact is likely to be a consequence of the charge correlations in an IL and requires the use of a generalized statistical thermodynamics. It has been observed that the ionic distribution in the vicinity of a strongly charged surface [25] and in the monolayer region of a monolayer protected nanocluster [26] Tsallis thermostatics can satisfactorily account for the charge correlations through a Tsallis entropic index $q < 1$ ($q = 1$ corresponds to the classical Boltzmann statistics). In a similar form as the Poisson–Boltzmann equation is modified in Tsallis thermostatistics by replacing the Boltzmann factor $e^{-\varepsilon/kT}$ by the Tsallis q-exponential [26,27], $e_q^{-\varepsilon/kT} \equiv \left[1-(1-q)(\varepsilon/kT)\right]^{1/(1-q)}$ we propose to replace the exponentials in Eq. (3) with the corresponding q-exponential.

Satisfactory agreement between the experiments results and the simulations was achieved by using a single value for the transfer coefficient α at each temperature. Moreover, the value obtained for the entropic index, $q = 0.8, \ldots, 0.9$, can be considered to be in agreement with previous finding in charge-correlated systems [25,26]. Although the description of the heterogeneous electron transfer kinetics in some other IL systems has not required the modification of the Butler–Volmer equation, it should be stressed that importance of the charge correlations vary from one system to another

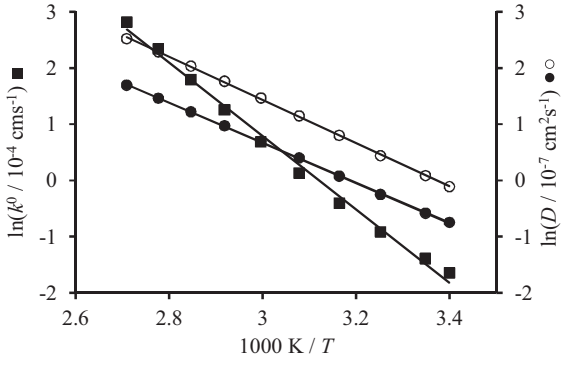

Fig. 7. Arrhenius plots of diffusion coefficients $D_{Cu(II)}$ (●) and $D_{Cu(I)}$ (○), and heterogeneous rate constant k^0 (■).

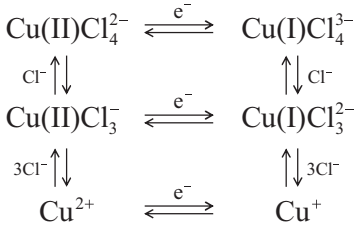

Scheme 1. Scheme-of-Squares used in attempt to explain the voltammograms.

Table 3
Fitted parameters at different temperatures using q-exponent, Eq. (4).

T (K)	$D_{Cu(II)}$ (10^{-7} cm^2 s^{-1})	$D_{Cu(I)}$ (10^{-7} cm^2 s^{-1})	k^0 (10^{-4} cm s^{-1})	α	q	$E^{0'}$ (mV)
294.2	0.49 ± 0.08	0.9 ± 0.2	0.14 ± 0.02	0.2874	0.908	739.8
298.7	0.57 ± 0.09	1.1 ± 0.2	0.19 ± 0.02	0.2809	0.911	745.0
307.5	0.8 ± 0.1	1.6 ± 0.3	0.32 ± 0.03	0.2716	0.917	751.6
316.1	1.1 ± 0.2	2.2 ± 0.4	0.56 ± 0.05	0.2575	0.919	760.6
324.9	1.5 ± 0.2	3.1 ± 0.5	0.98 ± 0.08	0.2398	0.918	770.9
333.8	2.0 ± 0.3	4.3 ± 0.7	1.7 ± 0.1	0.2185	0.907	782.2
342.7	2.6 ± 0.4	6 ± 1	3.1 ± 0.2	0.1956	0.883	795.0
351.3	3.4 ± 0.5	8 ± 1	5.2 ± 0.4	0.1757	0.855	807.6
360.2	4.2 ± 0.7	10 ± 2	8.8 ± 0.7	0.1579	0.827	820.9
369.1	5.2 ± 0.9	12 ± 2	14 ± 1	0.1532	0.808	835.6
Error				±0.0004	±0.003	±0.3
E_a kJ/mol	29.0 ± 0.2	31.7 ± 0.2	55.8 ± 0.9			
B	(6.8 ± 0.5) ×10^{-3} cm^2 s^{-1}	(3.9 ± 0.3) ×10^{-2} cm^2 s^{-1}	(10 ± 3) ×10^4 cm s^{-1}			

and that the value of q here obtained indicates a moderate deviation from the classical, low-coupling limit where the correlation can be neglected and Boltzmann statistics applies. In any case, this Tsallis-modified Butler–Volmer equation might be useful in future electrochemical studies on ILs. The q-exponential modified kinetic current in the fit is

$$-\frac{i}{FAk^0} = C_O^s e_q^{-\alpha f\eta} - C_R^s e_q^{(1-\alpha)f\eta} \quad (4)$$

and the results are shown in Table 3. The shapes of the fitted CSVs (not shown) are almost identical to the previous ones shown in Figs. 4–6.

The comparison of the results for the q-exponential fit in Table 3 with the non-conjugate ($\beta \neq 1-\alpha$) results in Table 2 shows that the diffusion coefficients are not significantly different, whereas the heterogeneous rate constant is smaller for the q-exponential fit. The activation energies are not significantly different between the two fits. Although not directly comparable, the transfer coefficients (α's) in both cases have the same declining behavior with increasing temperature, the q-exponential fit giving slightly larger values.

3.3. Constant current electrolysis of chloride solutions

In a constant current experiment, the surface concentration of an electroactive species drops to zero at the transition time τ, which can be seen as a rapid change in the cell potential. With metal electrodes in aqueous solutions, the electrode potential easily drifts to the water splitting region but this problem does not occur in ILs. The diffusion coefficient D of the electroactive species (see Appendix A) can be calculated from its transition time τ via the Sand equation

$$\frac{i\sqrt{\tau}}{c^b} = \frac{nFA\sqrt{D\pi}}{2} \quad (5)$$

In Eq. (5) i is the applied current, n the number of electrons transferred, F the Faraday constant, A the electrode area and c^b the bulk concentration of the electroactive species. The Sand equation is valid also under kinetic control of the current, only the electrode potential then increases due to the activation overpotential. If homogeneous kinetics [28] or natural convection intervenes, the Sand equation is naturally not valid.

In the constant current experiments with $BMPTf_2N$ electrolytes containing BMPCl, the electrode reaction was the oxidation of free chloride to chlorine (n = 1 in Eq. (5)). A copper block with several cylindrical compartments of 5 mm depth and 5 mm diameter was used as an electrolyte container; it also worked as an auxiliary electrode. To reduce problems involving preconditioning and chlorine poisoning, the working electrode was removed from the container between each measurement, wiped clean, and placed in a compartment containing fresh electrolyte. A two-electrode setup was used because the uncompensated ohmic resistance has virtually no effect on the transition time. The transition times were determined using the internal analysis tool of GPES measurement software. In the c^b = 77 mM BMPCl electrolyte (Fig. 8a), oxidizing currents of 1.7 μA, 6.5 μA, 8.5 μA, 11.0 μA, and 30.0 μA were applied, and in the 184 mM BMPCl electrolyte (Fig. 8b), oxidizing currents of 4.0, 15.0, 20.0, 25.0, and 30.0 μA were applied. The E–t graphs for the lowest currents in both electrolytes were recorded at 100 ms resolution and the rest at 1 ms resolution fast mode. The currents below 30.0 μA were chosen so that the transition times were of the same order of magnitude, making the comparison between the two chloride electrolytes easier.

Fig. 9 shows that the product $i\sqrt{\tau}/c^b$ from Fig. 8 remains constant with i, proving that chloride is directly oxidized without a preceding reaction [28]. Furthermore, it also indicates that the diffusion coefficient D does not vary significantly as a function of the concentration. Error bars can be drawn estimating an error of 0.01 s for the transition time, 0.1 μA for the current, and using the errors for the two concentrations calculated previously. The reason why the error bars vary without an obvious trend is that the errors of each term in the product $i\sqrt{\tau}/c^b$ are not of equal order. The final

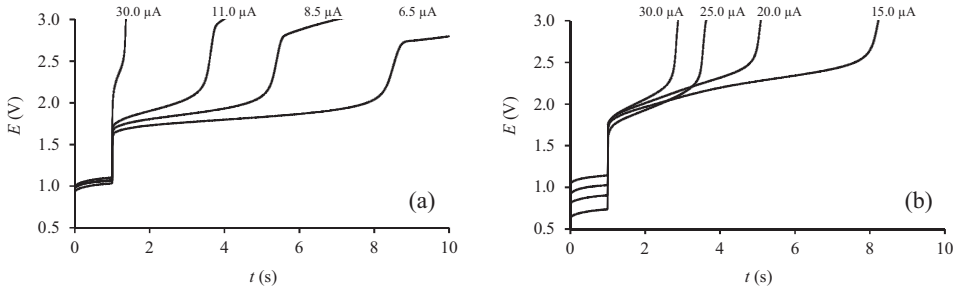

Fig. 8. E–t curves measured in the 77 mM (a) and in 184 mM BMPCl (b) electrolyte. Current is switched on at t = 1.0 s.

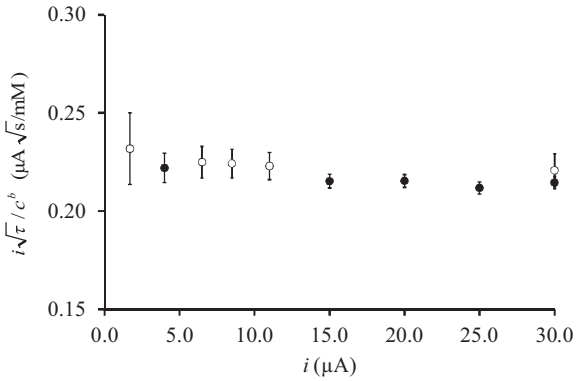

Fig. 9. Test of the Sand equation for the oxidation of chloride in two different concentrations: 77 mM (○) and 184 mM (●) of BMPCl in $BMPTf_2N$.

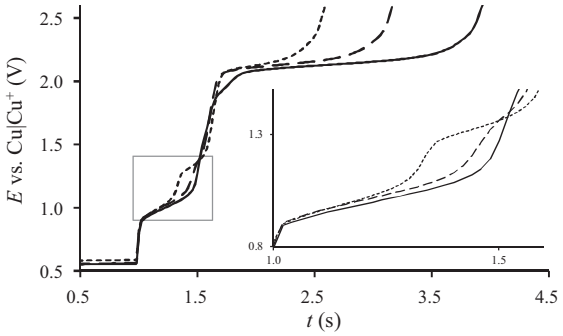

Fig. 11. Potential-time responses at 30.0 μA constant current in three 0.1 M Cu(I) electrolytes with different total chloride concentration: 392 mM (- - -), 435 mM (— — —), 480 mM (——). Current is switched on at $t = 1.0$ s.

result for the product $i\sqrt{\tau}/c^b$ is taken as a mean, weighted with the error bars, which obviously biases the result toward the values obtained using the higher concentration (184 mM) and the highest currents. The value is thus $0.216 \pm 0.002\ \mu A\ s^{1/2}/mM$. The diffusion coefficient of chloride can be calculated using the Sand equation (5). Using an error of 10 μm for the electrode diameter, D_{Cl^-} is $(1.03 \pm 0.06) \times 10^{-7}\ cm^2\ s^{-1}$ at $26 \pm 1\ ^\circ C$.

3.4. Constant current electrolysis of the Low Cu(I) solutions

Fig. 10(a) shows the potential–time curves measured in the Low Cu(I) electrolyte, i.e. oxidation of Cu(I) to Cu(II), and the corresponding plot of $i\sqrt{\tau}/c^b$ vs. i. Oxidizing currents were employed in the range from 0.75 μA to 30.0 μA. The open circuit potential of the cell was initially around 0.25 V, but it was returned to approximately 0.45 V by mixing after an oxidizing constant current experiment, which provided sufficient reproducibility. The transition times were measured using the same three-electrode cell setup in which the cyclic voltammograms were recorded. Because iR-compensation is of no concern in transition time measurements, potentials were recorded against the copper capillary reference electrode filled with the Low Cu(I) electrolyte. Measurements with $\tau > 100$ s must be disregarded, apparently due to the onset of natural convection. This perturbation can also be seen increasing to a lesser extent between currents from 1.0 μA to 5.0 μA. Therefore, the value of $i\sqrt{\tau}/c^b$ for Cu(I) oxidation is taken as a weighted mean from values obtained using the highest currents between 10.0 μA and 30.0 μA. In a similar manner, as with the oxidation of chloride in Fig. 9, the error bars have been drawn in Fig. 10(b), estimating an error of 0.01 s for the transition time. The final value of $i\sqrt{\tau}/c^b$ is $(0.236 \pm 0.006)\ \mu A\ s^{1/2}/mM$. The diffusion coefficient of Cu(I) can be calculated using the Sand Eq. (4) as $D_{Cu(I)}$ is $(1.23 \pm 0.11) \times 10^{-7}\ cm^2\ s^{-1}$ at $(26 \pm 1)^\circ C$, which is in good agreement with the value obtained from fitting the CSVs, $(1.1 \pm 0.2) \times 10^{-7}\ cm^2\ s^{-1}$ at 25.5 °C.

3.5. Constant current electrolysis of the High Cu(I) solutions

Following the successful analysis of the chloride electrolyte, and the low Cu(I) concentration electrolyte, the results can now be used to analyze the High Cu(I) electrolytes. Transition times were measured using the same two-electrode setup and measurement procedure as for the chloride solutions. An oxidizing current of 30 μA was applied, and the E–t data was recorded at 1 ms resolution in each High Cu(I) electrolyte. The combined oxidation of both the Cu(I) species and chloride can be seen in Fig. 11. The onset potentials for oxidations seen below 1.5 V in Fig. 11 are in excellent agreement with their voltammetric counterparts in Fig. 2. Both CSV and current step indicate the same potential range for Cu(I) oxidation (0.8 V). The potential of chloride oxidation at ca. 2.1 V is also consistent with previous results (Fig. 8). At the lowest chloride concentration, the extra wave is seen even in the constant current experiment. Determination of the transition time of the other Cu(I) complex with sufficient accuracy is, however, rather difficult, because its concentration is relatively low.

Table 4 shows the transition times in each electrolyte determined from the 1st oxidation wave corresponding to Cu(I), at ca. 0.8 V, and the 3rd oxidation wave corresponding to Cl^- oxidation, at ca. 2.1 V. Since D_{Cl^-} was obtained from the first set of experiments (Fig. 9), the concentration of free Cl^- can be calculated from the transition times of the 3rd waves in Fig. 11. Similarly, since $D_{Cu(I)}$ was determined in the second set of experiments (Fig. 10), the concentration of the 'first' Cu(I) complex oxidized at ca. 0.6 V can be also calculated. The error of the electrode area is canceled by using the product $i\sqrt{\tau}/c^b$ instead of the diffusion coefficient. Results are given in Table 4; an error of 0.1 μA has been estimated for the current.

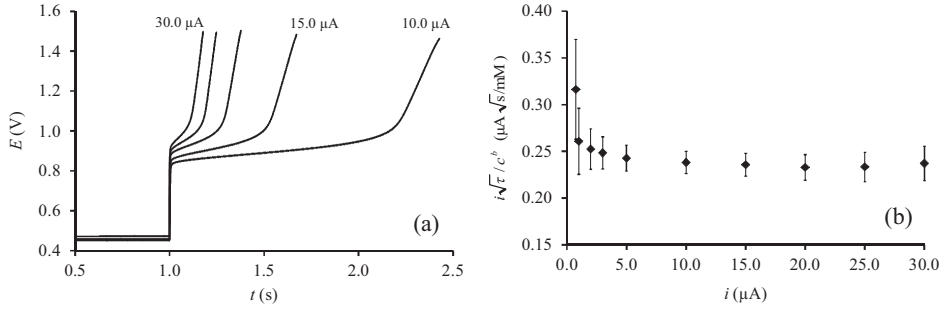

Fig. 10. (a) Potential–time curves measured in the Cu(I) electrolyte. Current (10.0–30.0 μA) is switched on at $t = 1.0$ s. (b) $i\sqrt{\tau}/c^b$ vs. i for oxidation of Cu(I). Measurements with 0.75, 1.0, 2.0, 3.0 and 5.0 μA currents are included to show that the Sand equation is not valid for such long experiments (at 1.0 μA, $\tau = 140$ s).

Table 4
Transition times measured for oxidations of Cu(I) and Cl^-, calculated values of $i\sqrt{\tau}$ and the calculated concentrations of the 'major' Cu(I) complex and free Cl^-.

$[Cl^-]_{tot}$ (mM)	$[Cu]_{tot}$ (mM)	Cu(I) oxidation τ/s	Cl^- oxidation τ/s	Cu(I) oxidation $i\sqrt{\tau}/\mu As^{1/2}$	Cl^- oxidation $i\sqrt{\tau}/\mu As^{1/2}$	$[Cu]_{major}$ (mM)	$[Cl^-]_{free}$ (mM)
392 ± 2	92 ± 2	0.30 ± 0.01	0.78 ± 0.01	16.5 ± 0.3	26.4 ± 0.3	71 ± 2	123 ± 2
435 ± 2	92 ± 2	0.41 ± 0.01	1.37 ± 0.01	19.1 ± 0.3	35.1 ± 0.2	82 ± 2	163 ± 2
480 ± 2	93 ± 2	0.47 ± 0.01	2.08 ± 0.01	20.6 ± 0.3	43.2 ± 0.2	88 ± 2	201 ± 3

A simple mass balance calculation using the values in Table 4 for the highest total chloride concentration (480 mM) reveals that multiplying the total concentration of copper by three (thus assuming all copper exists as $Cu(I)Cl_3^{2-}$ and subtracting the result from the total chloride concentration gives the remaining "free" chloride concentration (480 mM–3 × 93 mM), (201 ± 8) mM, in good agreement with the measured value (201 ± 3 mM). This does not rule out the possibility that two Cu(I) species can be present in other electrolyte solutions. Therefore, it is pertinent to investigate the mass balance considering the complexes $Cu(I)Cl_l^{1-l}$ and $Cu(I)Cl_l^{1-m}$, where l is the coordination number of the major species and m the coordination number of the minor species. The ratio between the amount of bound chloride calculated, on the one hand, by subtracting the free chloride concentration from the total chloride concentration, and calculated, on the other hand, from the coordination numbers in the complexes is

$$R = \frac{[Cl^-]_{tot} - [Cl^-]_{free}}{l \cdot [Cu]_{major} + m([Cu]_{tot} - [Cu]_{major})} \quad (6)$$

The value $R = 1.0$ indicates a correct chloride mass balance. Fig. 12 shows the ratios R calculated for the different total chloride concentrations indicated in Table 4 using different "l–m" chemical schemes. As an example, in a "3–2" scheme, $l = 3$ and $m = 2$.

Fig. 12 shows that the mass balance can only be satisfied if the major species is $Cu(I)Cl_3^{2-}$ (that is, $l = 3$). It is thus concluded that Cu(I) is mostly as a three coordinated chlorocomplex in the studied concentration range. Another supporting fact is that there is only one oxidation wave seen for Cu(I) at the highest chloride concentration (480 mM) in Fig. 11. In this concentration, the ratio R takes value closest to unity in the "3–2" and "3–3" coordination schemes, which is also true for the other concentrations. The "3–2" scheme is more plausible, because the increasing chloride concentration would favor the formation of $Cu(I)Cl_3^{2-}$ over $Cu(I)Cl_2^-$. The schemes "3–3" and "3–4" would not explain the disappearance of the second oxidation wave in Figs. 2 and 11 when the total chloride concentration is increased. Hence, in the studied molar ratio range ($[Cl^-]/[Cu(I)] < 8$) and ambient temperature the dominant chloride complex must be $Cu(I)Cl_3^{2-}$.

It must be realized that in the systems studied above, exact forms of the transport equations are, difficult to assess due to the ion-pairing, the degree of which is not known, or without the knowledge of the exact composition of the species present in the system. Therefore, the values of the transport parameters must be considered only as apparent, which is, however, sufficient for analytical or practical purposes and in, say, metal deposition from ILs. Yet, looking at Fig. 9, for example, it is clear that errors possibly made in the analysis are practically insignificant or canceled out.

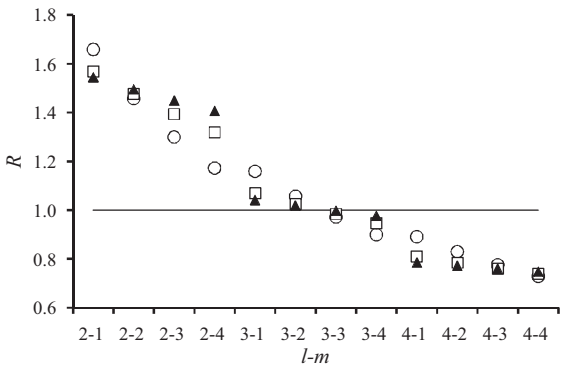

Fig. 12. Values of the ratio R (Eq. (6)) calculated for total Cl^- concentrations of 392 mM (○), 435 mM (□), and 480 mM (▲) in different coordination schemes "l–m".

4. Conclusions

The mass transport constants and kinetic parameters of electron transfer for copper chlorides in the RTIL $BMPTf_2N$ in the presence of a complexing salt BMPCl were determined. The mass transfer was studied with constant current electrolysis, and the results were in agreement with cyclic staircase voltammetry. Allowing the charge transfer coefficients α and β of the Butler–Volmer kinetics to be independent of each other, viz. $\beta \neq 1 - \alpha$, the measured cyclic voltammograms were fitted accurately. Simultaneous fitting of multiple data with different oxidation states for copper showed that the system is quasi-reversible and that the diffusion coefficient for Cu(I) is significantly higher than for Cu(II). Deviation of the charge transfer coefficients from a single value of α could be explained using the non-excessive Tsallis' thermodynamics.

The method of reacting Cu(II) with solid Cu through comproportionation proved to be an efficient method for making Cu(I) electrolytes, as the conversion appeared to be complete in all applied electrolytes. The number of the coordinating chloride ions of the dominant Cu(I) species was determined to be three. Evidence of a second copper complex was also presented. Such information is crucial in controlling the chemistry of coordinating compounds in RTILs. Knowing the requirements to maintain a certain degree of complexation, or the mere knowledge of the possibility of multiple prevailing species, is key to controlling and analysing the electrochemistry of any system.

Acknowledgements

The authors would like to thank Professor Elisabet Ahlberg from the University of Göteborg for discussing the coordination chemistry of metal chlorides, and Hannu Revitzer for AAS analysis. The Finnish Funding Agency for Technology and Innovation (TEKES) and Outokumpu Foundation are acknowledged for funding. J.A.M. thanks the Generalitat Valenciana (project no. PROMETEO/2012/069) and the Ministry of Science and Innovation of Spain and FEDER (project no. MAT2009-07747) for financial support.

Appendix A.

A.1. Simulation of Fig. 1

To prove that Fig. 1 can be, indeed reproduced by the slow homogeneous reaction, a simulation was done with the following parameter values: $D_1 = 6 \times 10^{-8}\ cm^2\ s^{-1}$, $D_2 = 10^{-7}\ cm^2\ s^{-1}$, $D_3 = 5 \times 10^{-8}\ cm^2\ s^{-1}$, $D_4 = 9 \times 10^{-8}\ cm^2\ s^{-1}$, $D_5 = 10^{-7}\ cm^2\ s^{-1}$, $K = k_1/k_2 = 25\ dm^3/mol$, $[Cl]_T = 0.092$ mM, $[Cl]_T = 0.392$ mM, thickness of the unstirred layer 4 μm, $E_1^0 = 600$ mV, $E_2^0 = 400$ mV. Subscript 1 is used for $Cu(I)Cl_2$ complex, 2 for $Cu(I)Cl_3$ complex, 3 for $Cu(II)Cl_2$ complex and 4 for $Cu(II)Cl_3$ complex, and 5 for free

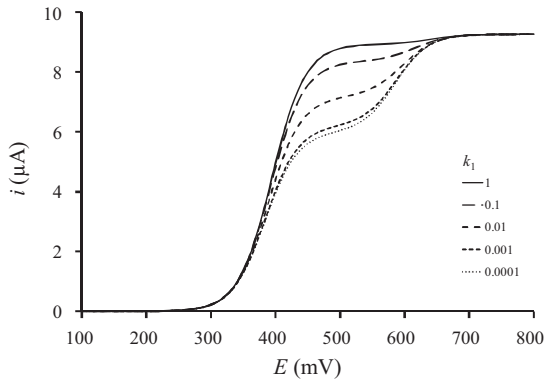

Fig. A1. Simulation of Fig. 1 The unit of k_1 is $dm^3\ mol^{-1}\ s^{-1}$. Scan rate is 2 mV/s.

chloride; k_1 is the second order homogeneous rate constant for Cl^- addition and k_2 the first order constant for its removal. The electrode reactions are assumed reversible. Hence, if $k_1 = 0.001, \ldots, 0.01\ dm^3\ mol^{-1}\ s^{-1}$, the voltammogram looks similar to Fig. 1 (Fig. A1 and Scheme A1).

A.2. Transport equations in ILs

The use of the Nernst–Planck or Fick's equations in ILs needs some consideration because the ionic liquid participates in carrying electric current, and because the number and meaning of the diffusion coefficients has to be clarified. For instance, a pure IL consisting of a cation A^+ (species 1), an anion B^- (species 2) is a single component system from the point of view of thermodynamics. Then, by definition, no diffusion process can take place and the only transport coefficient is the electrical conductivity of the pure IL. Since the ionic flux densities must satisfy the condition $M_1 j_1 + M_2 j_2 = 0$ in the barycentric reference frame, the mobility of one ionic species and its contribution to the total conductivity are inversely proportional to its molar mass.

The constant current experiments reported in Figs. 8 and 9 have been done in a binary system IL–salt where the salt has a cation A^+ in common with the IL and a different anion Cl^- (species 3). In this binary system, the local electroneutrality condition $c_1 = c_2 + c_3$ and the Euler equation $c_1\upsilon_1 + c_2\upsilon_2 + c_3\upsilon_3 = c_{12}\upsilon_{12} + c_{13}\upsilon_{13} = 1$, where c_i and υ_i are the molar concentration and molar volume of species i ($i = 1, 2, 3$ or 12, 13), imply that the three ionic concentration gradients can be written in terms of a single electrolyte concentration gradient

$$\frac{dc_3}{dx} = \frac{dc_{13}}{dx}, \quad \frac{dc_2}{dx} = \frac{dc_{12}}{dx} = -\frac{\upsilon_{13}}{\upsilon_{12}}\frac{dc_{13}}{dx}, \quad \frac{dc_1}{dx} = \frac{dc_2}{dx} + \frac{dc_3}{dx} = \frac{\upsilon_{12} - \upsilon_{13}}{\upsilon_{12}}\frac{dc_{13}}{dx}. \tag{A.1}$$

The flux densities (in the barycentric reference frame) must satisfy the condition

$$M_1 j_1 + M_2 j_2 + M_3 j_3 = M_{12} j_{12} + M_{13} j_{13} = 0 \tag{A.2}$$

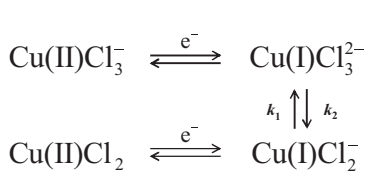

Scheme A1. Scheme of reactions used to simulate Fig. 1.

where M_i is the molar mass of species i ($i = 1, 2, 3$ or 12, 13), and therefore $j_{12} = -j_{13}M_{13}/M_{12}$. Thus, the ionic flux densities can be presented in the diffusion–conduction form [29] as

$$j_1 = j_{12} + j_{13} + t_1\frac{I}{F} = \frac{M_2}{M_{12}}\frac{I}{F} + \left(1 - \frac{M_{13}}{M_{12}}\right)j_3$$
$$j_2 = j_{12} - t_2\frac{I}{F} = -\frac{M_1}{M_{12}}\frac{I}{F} - \frac{M_{13}}{M_{12}}j_3 \tag{A.3}$$
$$j_3 = j_{13} - t_3\frac{I}{F} = -D\frac{dc_{13}}{dx} - t_3\frac{I}{F}$$

where t_i is the (local migrational) transport number of species i ($i = 1, 2$ and 3). The diffusion coefficient D actually characterizes the interdiffusion of the two components although it is customary to refer to D as the diffusion coefficient of ionic species 3. Obviously, Eq. (A.3) satisfy the equation of the conduction electric current density

$$j_1 - j_2 - j_3 = \frac{I}{F} \tag{A.4}$$

and the transport numbers satisfy $t_1 + t_2 + t_3 = 1$ and $M_1 t_1 - M_2 t_2 - M_3 t_3 = 0$.

The three independent transport coefficients of this system, (D, t_3 and electrical conductivity κ) can be related to the three friction coefficients in the Stefan–Maxwell formalism [30], which is maybe more appropriate to describe the transport processes in the IL,

$$c_1\nabla\tilde{\mu}_1 = c_1\nabla\mu_1 + c_1F\nabla\phi = K_{1,2}(\upsilon_2 - \upsilon_1) + K_{1,3}(\upsilon_3 - \upsilon_1)$$
$$c_2\nabla\tilde{\mu}_2 = c_2\nabla\mu_2 - c_2F\nabla\phi = K_{1,2}(\upsilon_1 - \upsilon_2) + K_{2,3}(\upsilon_3 - \upsilon_2), \tag{A.5}$$
$$c_3\nabla\tilde{\mu}_3 = c_3\nabla\mu_3 - c_3F\nabla\phi = K_{1,3}(\upsilon_1 - \upsilon_3) + K_{2,3}(\upsilon_2 - \upsilon_3)$$

where c_i and $\tilde{\mu}_i$ are the molar concentration and electrochemical potential of species i, $K_{i,j}$ is the friction coefficient between species i and j, and $\upsilon_i = j_i/c_i$ is the velocity of species i. It is thus obtained after lengthy algebra that

$$\kappa = F^2\frac{K_{2,3}(c_1)^2 + K_{1,3}(c_2)^2 + K_{1,2}(c_3)^2}{K_{1,2}K_{1,3} + K_{1,2}K_{23} + K_{1,3}K_{23}}$$
$$t_3 = \frac{K_{1,2}(c_3)^2}{K_{2,3}(c_1)^2 + K_{1,3}(c_2)^2 + K_{1,2}(c_3)^2} \tag{A.6}$$
$$D = \frac{M_{12}c_1}{M_{12}c_2 + M_{13}c_3}\frac{t_3(c_2)^2}{K_{1,2}}\left[\frac{\upsilon_{13}}{\upsilon_{12}}\left(\frac{\partial\mu_2}{\partial c_2}\right)_{T,p} + \left(\frac{\partial\mu_3}{\partial c_3}\right)_{T,p}\right].$$

The conductivity is obtained from the definition [29]

$$I = -\kappa\left(\nabla\phi + \frac{1}{F}\sum_{i=1}^{3}\frac{t_i}{z_i}\nabla\mu_i\right) = -\kappa(\nabla\phi - \nabla\phi_{dif}), \tag{A.7}$$

t_3 is found from its definition as the relative contribution of species 3 to the conductivity, and D is obtained by solving for $\upsilon_2 - \upsilon_1 = j_2^1/c_2$ and $\upsilon_3 - \upsilon_1 = j_3^1/c_3$ from Eq. (A.5), and noticing that $(t_2 + x_2t_1)j_3^1 - (t_3 + x_3t_1)j_2^1 = x_2j_{13} - x_3j_{12}$, where $x_2 = 1 - x_3 = c_2/c_1$. It is worth noticing that D depends on the composition and the molar masses and volumes of the electrolytes.

If species 3 (Cl^-) is a trace ion, $c_3 \ll c_2$, it becomes clear from Eq. (A.6) and (A.3) that $t_3 \approx 0$ and the flux density of species 3 can be described by Fick's law, $j_3 \approx -D\mathrm{d}c_{13}/\mathrm{d}x$, where $D \approx RTc_{13}/(K_{2,3} + K_{1,3})$ can be considered approximately independent of c_{13}, because $c_{13} \propto K_{2,3} + K_{1,3}$. The equations derived in this Appendix justify the use of Sand's equation in the analysis of experimental data and provide a clear meaning to the diffusion coefficient D.

All the other experiments with Cu complexes are done in a ternary system, which makes the derivations above quite tedious, but the basic message remains the same: at trace concentrations the

use of Fick's law is justified, but the diffusion coefficients depend on the composition of the system.

References

[1] D.R. MacFarlane, P. Meakin, J. Sun, N. Amini, M. Forsyth, Pyrrolidinium imides: a new family of molten salts and conductive plastic crystal phases, Journal of Physical Chemistry B 103 (1999) 4164.

[2] S. Zein El Abedin, N. Borisenko, F. Endres, Electrodeposition of nanoscale silicon in a room temperature ionic liquid, Electrochemistry Communications 6 (2004) 510.

[3] N. Borisenko, S. Zein El Abedin, F. Endres, *In situ* stm investigation of gold reconstruction and of Silicon electrodeposition on Au(1 1 1) in the room temperature ionic liquid 1-butyl-1-methylpyrrolidinium bis(trifluoromethylsufonyl)imide, Journal of Physical Chemistry B 110 (2006) 6250.

[4] S. Zein El Abedin, E.M. Moustafa, R. Hempelmann, H. Natter, F. Endres, Additive free electrodeposition of nanocrystallinealuminium in a water and air stable ionic liquid, Electrochemistry Communications 7 (2005) 1111.

[5] S. Zein El Abedin, E.M. Moustafa, R. Hempelmann, H. Natter, F. Endres, Electrodeposition of nano- and microcrystalline Aluminium in three different air and water stable ionic liquids, ChemPhysChem 7 (2006) 1535.

[6] S. Zein El Abedin, H.K. Farag, E.M. Moustafa, U. Welz-Biermann, F. Endres, Electroreduction of tantalum fluoride in a room temperature ionic liquid at variable temperatures, Physical Chemistry Chemical Physics 7 (2005) 2333.

[7] S. Zein El Abedin, A.Y. Saad, H.K. Farag, N. Borisenko, Q.X. Liu, F. Endres, Electrodeposition of selenium, indium and copper in an air- and water-stable ionic liquid at variable temperatures, Electrochimica Acta 52 (2007) 2746.

[8] P.-Y. Chen, I.-W. Sun, Electrochemical study of copper in a basic 1-ethyl-3-methylimidazolium tetrafluoroborate room temperature molten salt, Electrochimica Acta 45 (1999) 441.

[9] K. Murase, K. Nitta, T. Hirato, Y. Awakura, Electrochemical behaviour of copper in trimethyl-n-hexylammonium bis((trifluoromehyl)sulfonyl)amide, an ammonium imide-type room temperature molten salt, Journal of Applied Electrochemistry 31 (2001) 1089.

[10] C.L. Hussey, L.A. King, R.A. Carpio, The Electrochemistry of copper in a room temperature acidic chloroaluminate melt, Journal of the Electrochemical Society 126 (1979) 1029.

[11] C. Nanjundiah, R.A. Osteryoung, Electrochemical studies of Cu(I) and Cu(II) in an aluminum chloride-N(n-Butyl)pyridinium chloride ionic liquid, Journal of the Electrochemical Society 130 (1983) 1312.

[12] T.M. Laher, C.L. Hussey, Copper(I) and Copper(II) Chloro Complexes in the basic aluminum chloride-1-methyl-3-ethylimidazolium chloride ionic liquid, Inorganic Chemistry 22 (1983) 3247.

[13] T. Vainikka, Electrodeposition of metals from ionic liquids, Master's Thesis, Helsinki University of Technology, 2008.

[14] H. Matsuda, Y. Ayabe, Zur theorie der randles-sevčikschen kathodenstrahlpolarographie, Zeitschrift fur Elektrochemie 59 (1955) 494.

[15] R.S. Nicholson, Theory and application of cyclic voltammetry for measurement of electrode reaction kinetics, Analytical Chemistry 37 (1965) 1351.

[16] J.H. Christie, P.J. Lingane, Theory of staircase voltammetry, Journal of Electroanalytical Chemistry 10 (1965) 176.

[17] M.M. Murphy, J.J. O'Dea, D. Arn, J.G. Osteryoung, Theory of cyclic staircase voltammetry for electrode kinetics, Analytical Chemistry 61 (1989) 2249.

[18] M.D. Ryan, Cyclic staircase voltammetry, Journal of Electroanalytical Chemistry Interfacial Electrochemistry 79 (1977) 105.

[19] M. Galassi, et al., GNU Scientific Library Reference Manual, 3rd ed., 2010, ISBN 0954612078.

[20] D. Britz, Digital Simulation in Electrochemistry, Second, in: Revised and Extended Edition, Springer-Verlag, Berlin Heidelberg, 1988.

[21] J. Villadsen, M.L. Michelsen, Solution of Differential Equation Models by Polynomial Approximation, Prentice-Hall Inc, New Jersey, 1978.

[22] E. Fehlberg, Low-Order Classical Runge-Kutta Formulas With Stepsize Control and their Application to Some Heat Transfer Problems, NASA TR R-315, National Aeronautics and Space Administration, Washington, DC, 1969.

[23] J. O'Dea, J. Osteryoung, T. Lane, Determining kinetic parameters from pulse voltammetric data, Journal of Physical Chemistry 90 (1986) 2761.

[24] J. Osteryoung, Voltammetry for the future, Accounts of Chemical Research 26 (1993) 77.

[25] V. Garcia-Morales, J. Cervera, J. Pellicer, Coupling theory for counterion distributions based in Tsallis statistics, Physica A 339 (2004) 482.

[26] V. Garcia-Morales, S. Mafé, Monolayer-protected metallic nanoparticles: limitations of the concentric sphere capacitor model, Journal of Physical Chemistry C 111 (2007) 7242.

[27] L.M. Varela, J. Carrete, R. Muñoz-Solá, J.R. Rodríguez, J. Galledo, Nonextensive statistical mechanics of ionic solutions, Physics Letters A 370 (2007) 405.

[28] P. Delahay, T. Berzins, Theory of Electrolysis at Constant Current with Partial or Total Control by Diffusion- Application to the Study of Complex Ions, Journal of the American Chemical Society 75 (1953) 2486.

[29] K. Kontturi, L. Murtomäki, J.A. Manzanares, Ionic Transport Processes, Oxford University Press, Oxford, 2008.

[30] J.A. Wesselingh, R. Krishna, Mass Transfer in Multicomponent Mixtures, Delft University Press, Delft, 2000.